Published in final edited form as:
Nat Struct Mol Biol. 2013 May ; 20(5): . doi:10.1038/nsmb.2546.

Structural Basis of Signal Sequence Surveillance and Selection by the SRP-SR Complex

Ottilie von Loeffelholz[1,2], **Kèvin Knoops**[1,2,6], **Aileen Ariosa**[3,6], **Xin Zhang**[3,4], **Manikandan Karuppasamy**[1,2], **Karine Huard**[1,2], **Guy Schoehn**[1,2,5], **Imre Berger**[1,2], **Shu-ou Shan**[3,*], and **Christiane Schaffitzel**[1,2,*]

[1]European Molecular Biology Laboratory (EMBL), Grenoble Outstation, 38042 Grenoble, France

[2]Unit of Virus Host-Cell Interactions, Université Joseph Fourier (UJF)-EMBL-Centre National de la Recherche Scientifique (CNRS), UMI 3265, 38042 Grenoble, France

[3]Division of Chemistry and Chemical Engineering, California Institute of Technology, Pasadena, CA 91125, United States

[4]Department of Molecular and Experimental Medicine, The Scripps Research Institute, La Jolla, CA 90037, United States

[5]CNRS-CEA (Commissariat à l'énergie atomique et aux énergies alternatives)-UJF - Institut de Biologie Structurale-Jean-Pierre Ebel, UMR 5075, 38027 Grenoble, France

Abstract

Signal recognition particle (SRP)-dependent protein targeting to membranes is a multistep quality control process. Ribosomes translating weakly hydrophobic signal sequences can be rejected after SRP binding from the targeting reaction. Here, we show that the *early* targeting complex, formed by *Escherichia coli* SRP and its receptor FtsY with ribosomes translating the incorrect cargo EspP, is unstable and rearranges inefficiently into subsequent conformational states, such that FtsY dissociation is favoured over successful targeting. The N-terminal extension of EspP is responsible for these defects in the *early* targeting complex. The cryo-electron microscopic structure of this 'false' *early* complex with EspP reveals an ordered M-domain of Ffh (SRP protein) making two ribosomal contacts, and the NG-domains of Ffh and FtsY forming a distorted, flexible heterodimer. Our results provide a structural basis for SRP-mediated signal sequence selection during the recruitment of the SRP receptor.

INTRODUCTION

The universally conserved signal recognition particle (SRP) targets nascent proteins with hydrophobic signal sequences to translocation machineries at the target membrane[1–4].

*Correspondence should be addressed to: S.S., shan@caltech.edu; C.S., schaffitzel@embl.fr.
[6]These authors contributed equally to this work.

ACCESSION CODES

Protein Data Bank: The atomic model of SRP-FtsY in the 'false' *early* conformation has been deposited with accession code 3ZN8. The cryo-EM map has been deposited in the 3D–EM database under accession number EMDB-2316.

AUTHOR CONTRIBUTIONS

C.S., I.B, X.Z., and S.S designed experiments; C.S., K.H., O.V.L., A.A. and X.Z. performed sample preparations; A.A. and X.Z. carried out biochemical experiments; K.K., G.S. and M.K. performed the electron microscopy; O.V.L., M.K. and C.S. performed image analysis and model building; C.S., O.V.L., A.A., X.Z., and S.S. prepared the manuscript.

COMPETING FINANCIAL INTERESTS

The authors declare no competing financial interests.

Escherichia coli contains a minimal SRP consisting of the protein, Ffh (SRP54 homologue), and the 4.5S RNA which forms a stable hairpin structure with an evolutionary conserved tetraloop[5]. Ffh is composed of three domains: the N-terminal four-helix bundle and the GTPase domain that together form the functional NG-domain[6], as well as the M-domain which binds the 4.5S RNA and the hydrophobic signal sequence[7–9]. FtsY, the bacterial SRP receptor, also contains a NG-domain[10] preceded by an A-domain implicated in membrane and translocon (SecYEG in bacteria) binding[11,12]. The Ffh and FtsY NG-domains form a heterodimeric complex with a composite active site[13,14], in which GTP hydrolysis is activated without requiring an external GTPase activating protein.

During co-translational targeting, both the SRP and FtsY undergo sequential and discrete conformational states in the SRP-FtsY heterodimer, which have been characterized by fluorescence spectroscopy, mutational and structural analyses. First, SRP binds with high affinity and is retained longer on ribosomes with a nascent chain in the exit tunnel or exposing a hydrophobic signal sequence (RNC, cargo)[15,16]. In these cargo-SRP complexes, the Ffh NG-domain is positioned close to the SRP RNA tetraloop[17] which accelerates FtsY docking[18] and stabilizes the *early* SRP-FtsY targeting complex[19,20]. Subsequently, phospholipids and SecYEG drive GTP-dependent rearrangement from the transient *early* state, which lacks tight interaction between the Ffh-FtsY NG-domains, into the *closed* state[21,22]. Rearrangement into the *closed* state involves formation of a stable NG-domain complex with a continuous interface around the GTP molecules[13,14]. Subsequent GTPase activation involves optimization of the GTPase active site and relocation of the entire NG-domain complex to the opposite end of the SRP RNA (*activated* state)[22,23]. This drives the delivery of the cargo onto the SecYEG protein-conducting channel and the disassembly of the SRP-FtsY complex after GTP hydrolysis[24]. Throughout the targeting cycle, these GTPase rearrangements allow the SRP and FtsY to actively sense and respond to the presence of the cargo to achieve accurate temporal and spatial control[15,16,19].

In *E. coli*, the co-translational SRP pathway is mostly used for the integration of inner membrane proteins[25,26]. The hydrophobicity of the nascent chain is the main criterion for whether a nascent polypeptide is targeted co-translationally by the SRP pathway or post-translationally via SecA-SecB[26,27]. A threshold level of hydrophobicity appears to exist for SRP targeting because overexpression of the SRP cannot reroute a model substrate (maltose binding protein) from post- to co-translational targeting[27], indicating a high degree of specificity of the SRP pathway. More recent work suggests that the selection of cargos by the SRP is a multistep quality control process[15]. If “incorrect cargos” containing weak or no signal sequences are bound to the SRP, they can be rejected after FtsY docking as the SRP-FtsY complex undergoes sequential conformational changes during the delivery and unloading of cargo. Amongst them, a critical checkpoint is the *early* RNC-SRP-FtsY targeting complex, which is stabilized by at least a factor of 50 by a correct cargo compared to incorrect cargos or non-translating ribosomes[16,19].

A striking example for an “incorrect cargo” is the bacterial autotransporter EspP. The N-terminus of EspP comprises an unusual 55 amino acid signal sequence composed of a classical signal sequence and a N-terminal extension conserved among autotransporters [28,29] (Fig. 1a). *In vivo*, EspP is recognized by SRP, but translocated post-translationally using the SecA-B pathway[28]. *In vitro*, the RNC^{EspP} (RNC displaying the EspP signal sequence) is bound by the SRP with high affinity (13.6 nM)[15]. However, the *early* SRP-FtsY targeting complex formed in the presence of RNC^{EspP} yields a lower fluorescence resonance energy transfer (FRET) signal between donor-labeled Ffh and acceptor-labeled FtsY as compared to RNCs carrying strong signal sequences from *bona-fide* SRP substrates[15]. This indicates that the *early* targeting complex formed with RNC^{EspP} adopts a different structure than that formed with a strong SRP cargo, such as FtsQ (RNC^{FtsQ})[20].

To provide insights into the molecular mechanism of signal sequence selection by the SRP, we have determined the structure of the RNC^{EspP}-SRP-FtsY complex by single particle cryo-electron microscopy. By fitting the available high-resolution structures of the *E. coli* ribosome[30], the SRP[6–8,23,31] and FtsY[10] into the EM density, we generated a quasi-atomic model of the RNC^{EspP}-SRP-FtsY complex. This structure represents an unstable, 'false' *early* targeting complex, which is destined to be rejected from the SRP pathway. We identify functionally important differences in the conformation of the Ffh M- and NG-domains in the EM structure of this 'false' *early* targeting complex with RNC^{EspP} as compared to the RNC-SRP complex[17,32] and the *early* state complex formed with RNC^{FtsQ} [20]. Our structural data, underpinned by quantitative thermodynamic and kinetic analyses, provide a rationale for the rejection of this substrate from the SRP targeting pathway.

RESULTS

RNC-SRP binding alone cannot account for EspP rejection

We first asked whether deleting the N-terminal extension and increasing the hydrophobicity of the signal sequence may lead to a higher efficiency in the SRP-dependent targeting of EspP. To this end, the wildtype and three variants of the EspP signal sequence were fused to Prolactin as a model substrate, which is efficiently translocated across the membrane. One EspP signal sequence variant had the N-terminal extension of EspP deleted (EspPΔN), the second variant contained two leucine mutations (C42L G45L; EspP-Hydro), and the third variant comprised both of these alterations (EspPΔN-Hydro) (Fig. 1a). We measured the efficiency of SRP and FtsY to target these cargos in a heterologous *in vitro* protein targeting and translocation assay using microsomal membranes[33,34]. EspP was poorly translocated *in vitro* (Fig. 1b, Table 1 and Supplementary Fig. 1a), thus reproducing *in vivo* experiments[28]. Interestingly, increasing the hydrophobicity of the EspP signal sequence (EspP-Hydro) improved the translocation efficiency by less than a factor of two, whereas deletion of the N-terminal extension (EspPΔN and EspPΔN-Hydro) led to efficient targeting and translocation (Fig. 1b, Table 1), in agreement with previous observations *in vivo*[28]. These results strongly suggest that the N-terminal extension is the primary cause of the inefficient targeting of EspP.

We then asked whether deletion of the N-terminal extension improves the binding affinity of SRP for EspP cargos. As described earlier, RNC^{EspP} bound to SRP with moderate affinity (K_d ~13.6 nM; Fig. 1c, Table 1), comparable to that of another SRP-dependent substrate, 3A7L (LALLLLLALA), which is efficiently targeted[15]. Deletion of the N-terminal extension ($RNC^{EspP\Delta N}$) did not alter this binding affinity (Fig. 1c, Table 1). As expected, $RNC^{EspP\text{-}Hydro}$, which contains a highly hydrophobic signal sequence, bound to SRP strongly (K_d ~1.0 nM; Fig. 1c). Deletion of the N-terminal extension ($RNC^{EspP\Delta\text{–}Hydro}$) did not affect the SRP binding affinity either (Fig. 1c, Table 1). These results show that the N-terminal extension did not exert its inhibitory role on the SRP pathway by reducing the affinity between the SRP and the RNCs (Table 1). In light of these results and recent work[15], we hypothesize that the N-terminal extension of the EspP signal sequence interferes with subsequent steps of the SRP pathway, such as SRP-FtsY assembly.

EspP N-terminal extension leads to a distorted *early* complex

The SRP loaded with a correct cargo forms a stabilized RNC-SRP-FtsY *early* targeting complex, whereas incorrect cargos fail to provide this stabilization[15,16]. To test whether this were the case with EspP and its variants, we measured the stability of the *early* complex using FRET between DACM (donor)-labeled Ffh(C235) and BODIPY-FL (acceptor)-labeled FtsY(C487)[35]. The *early* targeting complexes formed with $RNC^{EspP\Delta N}$ and

$RNC^{EspP\Delta N–Hydro}$ were highly stable (Fig. 2a and Table 1), whereas inclusion of the N-terminal extension in the EspP signal sequence caused a reduction in the stability of the *early* targeting complexes formed with RNC^{EspP} and $RNC^{EspP\text{-}Hydro}$ (Fig. 2a, Table 1). In addition, the maximal FRET efficiencies of the *early* targeting complexes are 0.10–0.16 units lower with RNCs containing nascent chains with the N-terminal extension (Fig. 2a, Table 1), suggesting that the *early* targeting complex formed with RNC^{EspP} positions the SRP and FtsY GTPase domains differently from that with $RNC^{EspP\Delta N}$ or a correct SRP cargo.

Cryo-EM structure of the RNC^{EspP}-SRP-FtsY *early* complex

To gain insight into the nature of these differences, we determined the structure of the RNC^{EspP}-SRP-FtsY *early* targeting complex by single particle cryo-EM. To efficiently assemble the EspP *early* complex, we fused the C-terminus of FtsY to the N-terminus of Ffh via a 31-amino acid, glycine- and serine-rich linker (~117 Å). The resulting single-chain construct behaved similarly to the unlinked SRP and FtsY in ribosome binding and GTP hydrolysis experiments [20]. Importantly, a similar FtsY-SRP fusion was completely functional *in vivo* [36]. In co-sedimentation experiments, this single-chain SRP construct bound RNC^{EspP} equally well as RNC^{FtsQ} (Supplementary Fig. 1b). For cryo-EM, RNC^{EspP} complexes were incubated with a ten-fold excess of single-chain SRP construct in the absence of GTP to prevent subsequent rearrangements of the targeting complex, which may lead to additional conformational heterogeneity. After computational sorting and refinement (online Methods, Supplementary Fig. 2), the RNC^{EspP}-SRP-FtsY structure was reconstructed at 12 Å resolution (FSC 0.5 criterion) (Supplementary Fig. 3).

At the exit of the ribosomal tunnel, distinct elongated density was observed accounting for the SRP-FtsY complex (red in Fig. 2b), which had two connections to the large ribosomal subunit (50S; blue in Fig. 2b). A two-lobed density is positioned directly above the tunnel exit where the EspP nascent chain emerged. To generate a quasi-atomic model of the EspP *early* state, the crystal structures of the *E. coli* 70S ribosome [30], the *E. coli* SRP [6,8,23] and FtsY [10] were placed into the experimental density (Fig. 2c,d). The NG-domains of Ffh and FtsY were placed into the two-lobed density above the tunnel exit (Fig. 2c,d). The quasi-atomic model indicates that FtsY forms a contact with the 4.5S RNA tetraloop, which has been shown to stabilize FtsY binding to the SRP in the *early* complex (Fig. 2c,d)[20,37]. Although our single-chain construct of Ffh and FtsY contained the complete N-terminal A-domain of FtsY, this domain is not visible in our structure and thus is likely disordered. Notably, the complete M-domain of Ffh could be located in the density (Fig. 2c,d; see more discussions below). Two conformations of the signal sequence bound to the M-domain were reported[8,9]. In the quasi-atomic model, we included the structure fitting with the higher correlation coefficient[8]. We cannot exclude that the EspP signal sequence is bound slightly differently to the Ffh M-domain, as it is 35 residues longer than the 20 amino acid yeast dipeptyl aminopeptidase B signal sequence visible in the crystal structure[8]. Upon FtsY docking, the largest conformational change in the current structure when compared to the RNC^{FtsQ}-SRP complex[17] is the detachment of the Ffh N-domain from ribosomal protein L23 to contact the FtsY NG-domain (Supplementary Fig. 4).

M-domain is ribosome-bound in the RNC^{EspP}-SRP-FtsY complex

SRP recognition of a signal sequence leads to tight binding of the SRP to the RNC. In the RNC-SRP complex, the signal sequence is buried between the M-domain and the ribosome[17,32], and the M-domain is well-resolved forming contacts with rRNA helices h24 and h59 (Fig. 3a). In contrast, in the *early* targeting complex formed by RNC^{FtsQ} [20], the signal sequence-binding part of the M-domain detaches from h59, presumably without releasing the signal sequence, and is not visible in the EM reconstruction (Fig. 3b,

Supplementary Fig. 5). Only a single ribosomal contact remains involving the 4.5S–binding part of the M-domain and h24[20]. In the RNC^{EspP}-SRP-FtsY 'false' *early* complex, however, we found that the M-domain is ordered (Fig. 3c, Supplementary Fig. 5) and forms contacts to h24 and h59. This M-domain geometry resembles the M-domain conformation observed in the RNC^{FtsQ}-SRP complex devoid of FtsY (Fig. 3a,c,d). Thus, important rearrangements induced by the correct cargo that lead to a flexible M-domain[20] are not observed in the 'false' *early* complex.

The FtsY NG-domain interacts weakly with RNC^{EspP}-SRP

In the *early* targeting complex formed with RNC^{EspP}, the NG-domains of Ffh and FtsY are weakly associated (Fig. 4a) compared to the NG-domain arrangement observed in the crystal structures in which extensive contacts are formed between the two NG-domains[13,14]. Compared to the FtsQ *early* state (Fig. 4b), the Ffh NG-domain is closer to the M-domain (~16 Å) in the 'false' *early* complex. In our structure, the N-domain of Ffh contacts the N-domain and the NG-domain interface of FtsY. Overall, the NG-domain interaction is not very well defined (see below). In contrast, in the *early* complex formed with RNC^{FtsQ}, the Ffh-FtsY N-domains interact to form a pseudo-symmetric V-shaped complex (Fig. 4b,c)[20]. In both complexes, the G-domains are not involved in the interaction, and both GTPase active sites are accessible, consistent with the fact that the *early* complexes can form with or without nucleotides (Supplementary Fig. 1). In agreement with the FRET measurements (Fig. 2a), we observe a larger distance of the Ffh-FtsY G-domains (~68 Å) as compared to the FtsQ *early* complex (~60 Å)[20] and to the *closed* complex in which the G-domains interact tightly (31 Å)[13,14].

The FtsY NG-domain is tilted in the 'false' *early* complex, and the tip of the N-domain is displaced ~15 Å towards the Ffh NG-domain (Fig. 4c,d). The interaction between the FtsY G-domain and the RNA tetraloop is a major stabilizing interaction of the *early* targeting complex (Fig. 4b)[20,37]. The tilted conformation of the FtsY NG-domain in the EspP 'false' *early* complex likely weakens its interaction with the RNA tetraloop. Together with the weak interaction of the Ffh-FtsY NG-domains, this likely explains the low affinity of the *early* targeting complex formed with RNC^{EspP} (Fig. 2a, Table 1). In our EM structure, FtsY is covalently linked to Ffh by a flexible linker and therefore, this weak interaction is stabilized to prevent the disassembly of the complex.

We analyzed the structural heterogeneity of the SRP-FtsY in the 'false' *early* complex. The 3D variance map of the RNC^{EspP}-SRP-FtsY reconstruction indicates that the flexibility of the complex is highest in the Ffh-FtsY NG-domains (Supplementary Fig. 6). In comparison, the M-domain and the rRNA h59 are more rigid in this structure. We sorted for the SRP-FtsY heterogeneity in the 'false' *early* complex using 3D–classification by maximum-likelihood and multi-reference 3D angular refinement[38]. Maps showing differences in the SRP-FtsY part of the structure were used as input maps for supervised classification using the software Spider[39] resulting in two maps with clearly distinct SRP-FtsY conformations (Supplementary Fig. 7). Both structures contain the density for the M-domain, and a connecting density is visible between the Ffh NG-domain and the M-domain. The position of the Ffh NG-domain is different in the two structures. In one structure, the Ffh NG-domain is closer to the M-domain. In the second, the Ffh NG-domain moved away from the M-domain and is tilted such that the G-domain has a larger distance to the ribosome (Supplementary Fig. 7). Both conformations differ substantially from the pseudo-symmetric NG-domain arrangement observed in the *early* state (Fig. 4b)[20], underscoring multiple possibilities of how the NG-domains interact in the *early* state[40] depending on the nature of the nascent chain signal sequence.

Slow rearrangement of RNC^{EspP} to the *closed/activated* state

The less favorable Ffh-FtsY NG-domain arrangement observed in the RNC^{EspP} *early* complex likely impedes the formation of the stable *closed* complex, which is the subsequent step in the SRP pathway and required to deliver the RNC to the membrane[21]. Consistent with this hypothesis, RNC^{EspP} and RNC$^{EspP\text{-}Hydro}$ mediated the rearrangement from the *early* to *closed* complex at rate constants of 0.04 s^{-1} and 0.10 s^{-1}, respectively, which are slower than that previously observed with *bona-fide* SRP cargos by a factor of 3–7 (Fig. 5a, Table 1, Supplementary Table 1)[15]. When the N-terminal extension is deleted from EspP or EspP-hydro, this rearrangement occurred at faster rates, 0.13 s^{-1} and 0.18 s^{-1} respectively. Collectively, the lower stability of the *early* targeting complex (Fig. 2a, Table 1) and the slower *early*-to-*close* rearrangement (Fig. 5a) would lead to less efficient assembly of the *closed* complex, which is evidenced by direct measurements using a FRET assay: RNC^{EspP} and RNC$^{EspP\text{-}Hydro}$ mediated the assembly of the *closed* complex an order of magnitude slower than RNC$^{EspP\Delta N}$ and RNC$^{EspP\Delta N\text{-}Hydro}$ (Fig. 5b, Table 1).

DISCUSSION

Genetic, biochemical and structural analyses of the SRP and its receptor have led to considerable insight into the co-translational targeting cycle[2–4,41,42]. However, the molecular mechanism and structural details by which substrate proteins are surveyed and directed into the co- or post-translational targeting pathways have remained elusive to date. Here, we address this question using EspP, a secreted serine protease autotransporter with an unusually long, less hydrophobic signal sequence containing a basic N-terminal extension (Fig. 1a)[28,29,43], as a model substrate. EspP was chosen because RNCs translating EspP have been shown to interact well with the SRP *in vitro*[15], but EspP is targeted post-translationally *in vivo* [28]. We show that the N-terminal extension preceding the signal sequence causes EspP to be rejected from the SRP pathway *after* SRP binding. Our cryo-EM analysis of the RNC^{EspP}-SRP-FtsY 'false' *early* complex provides a structural basis for rejection of RNC^{EspP} from the SRP pathway.

Our results show that the basic N-terminal extension of the EspP signal sequence provides a strong 'SRP-avoidance' sequence that rejects substrate proteins from the SRP pathway. Even the EspP variant bearing a highly hydrophobic signal sequence is targeted poorly by the SRP in the presence of this extension. Interestingly, the N-terminal extension does not exert its inhibitory effect by disrupting high affinity binding of SRP to the RNC, as both RNC$^{EspP\text{-}Hydro}$ and RNC$^{EspP\Delta N\text{-}Hydro}$ bound the SRP with 1 nM affinity but were targeted with significantly different efficiency. Rather, this extension compromises the ability of RNCs to stimulate subsequent SRP-FtsY interactions, which are critical for completing the targeting cycle. In particular, SRP loaded with RNC^{EspP} or RNC$^{EspP\text{-}Hydro}$ forms a less stable and less productive *early* targeting complex with FtsY, leading to two consequences that disfavour the targeting reaction. First, FtsY dissociates more easily from a labile *early* targeting complex, requiring additional rounds of assembly and disassembly for the targeting reaction to proceed. Second, a distorted *early* targeting complex renders subsequent formation of a *closed/activated* RNC^{EspP}-SRP-FtsY complex slower. For these reasons, we term the *early* complex formed with RNC^{EspP} a 'false' *early* complex that is less conducive to complete a successful protein targeting reaction.

The cryo-EM structure of the RNC^{EspP}–SRP-FtsY complex reveals the structural origin of the unstable and non-productive 'false' *early* complex. Compared to the *early* complex with RNC^{FtsQ}, which adopts a pseudo-symmetric V-shaped SRP-FtsY NG-domain orientation, we observe in the RNC^{EspP} 'false' *early* complex a flexible, asymmetric heterodimer structure arrangement in which the N-domain of the SRP protein primarily interacts with the NG-domain interface of FtsY (Fig. 4a,c,d; Supplementary Fig. 7). Furthermore, the Ffh NG-

domain is displaced towards the M-domain, and the FtsY NG-domain is tilted towards Ffh. This likely results in a weaker interaction with the SRP RNA tetraloop, which is crucial for formation and stabilization of the *early* Ffh-FtsY complex[37,43]. Both effects may contribute to the lower affinity of the *early* targeting complex formed with RNC^{EspP} (K_d = 311 nM) as compared to those complexes formed with a strong SRP cargo (K_d ~40 nM) (Fig. 6). The conformational heterogeneity of the Ffh-FtsY NG-domain complex provides additional evidence for the lack of stable molecular interactions in the 'false' *early* complex. Moreover, it indicates that the incorrect cargo interferes with the formation of a pseudo-symmetric V-shaped NG-domain arrangement (Supplementary Fig. 7). Rearrangement into the stable, quasi-symmetric *closed* complex from this unfavourable and rather unstable NG-domain arrangement(s) would be more difficult, compared to a complex with properly prepositioned NG-domains.

An intriguing observation in this 'false' *early* complex is an ordered and visible Ffh M-domain forming two ribosomal contacts to rRNA helices 24 and 59. This arrangement resembles the ribosome-bound M-domain in the RNC-SRP structures in the absence of FtsY[17,32] where the signal sequence is buried between the M-domain and the ribosome. In contrast, in the *early* complex formed with a strong SRP cargo, the M-domain with the bound signal sequence became flexible[20], which likely represents a FtsY-induced rearrangement that ultimately leads to the release of the signal sequence from SRP and successful handover of the cargo to the translocon. It remains to be clarified whether the detachment of the M-domain is a prerequisite for a productive *early* state complex. The precise structural details of how the signal sequence bound M-domain communicates with the Ffh-FtsY NG-domains are still not understood. In principle, information could be transmitted from SRP to FtsY via the structurally flexible linker connecting the Ffh NG-domain with the M-domain or via the SRP RNA. Biochemical and structural data show that binding of the signal sequence to SRP induces an extensive conformational change that arranges the SRP RNA tetraloop to favorable positions for FtsY docking [17,20,37,43]. Concomitantly, this event requires a major reorientation of the linker to bring the Ffh NG-domain close to the tetraloop, which would be driven by productive interaction of the M-domain with a correct signal sequence on the ribosome, but not with an incorrect signal sequence. Our structure offers a first view of cargo-induced differences.

How does the N-terminal extension of EspP disrupt the *early* targeting complex? The N-terminal extension (EspP 1–25; Fig. 1) has a high propensity to form beta strand structures[44] One hypothesis is that this presents a steric block that prevents productive interaction of the SRP M-domain with the signal sequence. This could disrupt the communication between the M- and NG-domains of Ffh and thus lead to less productive interaction of Ffh with FtsY. Alternatively, the steric block from the EspP N-terminal extension could directly interfere with the formation of the NG-domain complex between Ffh and FtsY. The latter possibility is less likely, given that the NG-domain interface is at least 40 Å away from the hydrophobic core of the M-domain with the signal sequence.

The less favourable, non-symmetric NG-domain arrangement observed in the 'false' *early* state is likely responsible for its lower stability and slower rearrangement to the *closed* state observed biochemically. Thus, dissociation of the 'false' *early* complex will likely dominate over the delivery of RNC to the target membrane (Fig. 6). Moreover, translation of EspP continues during SRP targeting, and ribosomes with long nascent chains cannot be targeted efficiently via the SRP pathway to the membrane[45], imposing a limited time window for successful SRP-dependent targeting[45,46]. Incorrect signal sequences like EspP interfere with efficient SRP-FtsY *early* complex formation, and thereby render the targeting reaction to proceed too slowly and unlikely to be completed within this critical time window, thus resulting in their rejection from the co-translational targeting pathway. Similar observations

have been made with RNCs bearing other incorrect signal sequences, which are rejected at steps after the initial SRP binding, in part due to the unstable and unproductive *early* complex[15].

The SRP is present in all kingdoms of life. The mechanisms described here are obtained with prokaryotic SRP. Similar mechanisms are likely used by the eukaryotic SRP to reject incorrect substrate proteins. N-terminal extensions that act as 'SRP-avoidance' sequences are not unique to bacterial autotransporters like EspP. Several mitochondrial proteins contain extensions N-terminal to their first hydrophobic transmembrane domain [47]. These extensions effectively inhibit the nascent polypeptide from engaging the SRP pathway, and their deletion leads to efficient SRP-dependent targeting to the ER [47]. Presumably, these N-terminal extensions are important for directing the proteins to the mitochondria. Moreover, in a systematic screen of *Saccharomyces cerevisiae* SRP substrates, substantial binding of the SRP to nascent chains with neither transmembrane nor signal sequences was detected[48]. Nascent polypeptide-associated complex (NAC), which has overlapping substrate specificity with SRP *in vivo*, was suggested to improve the specificity of SRP in binding the correct cargos[49]; however, yeast cells lacking NAC do not suffer from increased protein mistargeting[48]. Given the evolutionary conservation of the SRP and its receptor, it is likely that highly similar surveillance mechanisms using induced fit and proofreading mechanisms exist also in eukaryotes to reject incorrect substrate proteins after initial SRP-RNC recognition.

ONLINE METHODS

Preparation of RNC^{EspP}-SRP-FtsY complexes

The plasmid pUC19StrepEspPSecM encodes for a N-terminal triple StrepII-tag, 88 amino acids of the EspP N-terminus with the signal sequence and 33 amino acids of the SecM C-terminus including the stalling sequence[15]. pUC19StrepEspPSecM was transcribed and translated *in vitro* using membrane-free cell extract as previously described[50]. Briefly, the ribosome-nascent chain complexes (RNCs) were purified by sucrose gradient centrifugation and affinity chromatography[50]. After centrifugation, the ribosomal pellet was dissolved in buffer A (50 mM Hepes-KOH, 100 mM KOAc, 8 mM $Mg(OAc)_2$, pH 7.5). To stabilize the SRP-FtsY complex, we used a construct in which full-size FtsY is linked to full-size Ffh via a 31 amino acid linker (corresponding to ~ 117 Å linker)[20]. The single-chain SRP-FtsY construct (scSRP) was purified by affinity purification via the hexahistidine-tag and anion exchange chromatography (MonoQ) as described before[20]. The complexes were reconstituted by incubation of 200 nM RNCs displaying the EspP nascent chain (RNC^{EspP}) with a 10-fold molar excess of scSRP for at least 60 min on ice. The binding of scSRP to RNC^{EspP} under these conditions was confirmed by co-sedimentation experiments through a 0.5 M sucrose cushion in buffer A (Supplementary Fig. 1).

Electron microscopy and image processing of RNC^{EspP}-SRP-FtsY complexes

Lacey carbon grids (Cu 300 mesh, Agar scientific) were glow discharged on both sides for 30 s, and 3 µl sample (200 nM RNCs) was applied on the carbon side. The grids were plunge frozen in liquid ethane using a Mark IV vitrification robot (FEI) after blotting for 1 s at 20 °C and 100% relative humidity. CCD frames were recorded under low-dose conditions on a Tecnai G2 Polara (FEI) operating at 300 kV and a specimen level magnification of 76,000x with a Gatan 4k x 4k CCD camera in a defocus range between −0.7 µm and −5.7 µm with an initial pixel size of 1.875 Å on the object scale.

The contrast transfer function (CTF) was determined and corrected with bctf (Bsoft package [51]). The CCD frames were re-sampled to 3.75 Å/pixel. A total number of 165,820

particles was selected semi-automatically from 1,974 CCD frames using e2boxer (EMAN2)[52]. The data were classified into four subsets according to ribosomal conformations, using low pass filtered ratcheted and not-ratcheted vacant ribosomes as initial references (EMDB IDs: 1363, 1056[53,54]), and SRP-FtsY complex presence in SPIDER (Supplementary Fig. 2)[39]. We also used maximum likelihood 3D refinement by XMIPP [38] on the complete dataset using a band-pass filtered 50S structure as initial reference to avoid bias in the sorting procedure[55]. However, the resulting three structures containing density corresponding to SRP-FtsY ultimately did not refine to the same resolution as with the approach described above. The pool of not-ratcheted RNC^{EspP}–SRP-FtsY complex contained 52,020 particles. Special care was taken not to have an overrepresentation of raw images in some of the class averages used for the reconstruction. Limiting the population of each class to the same number resulted in using 46,945 images for the final reconstruction. Full-size images were used for the last round of refinement. At the end of refinement, the data were split randomly to generate two reconstructions. These two independent reconstructions were then used for calculation of the FSC curve, and the resolution was assessed to be 12 Å by the Fourier shell correlation with a 0.5 threshold, and 8.3 Å according to the FSC 0.143 criterion[56] (Supplementary Fig. 3).

Analysis of Conformational Heterogeneity

The conformational heterogeneity of the RNC^{EspP}-SRP-FtsY complex was analyzed by maximum likelihood 3D refinement using mlf_refine3d (XMIPP[57]) and by hypergeometrically stratified resampling (HGSR) using SPARX[58].

For the 3D variance map of RNC^{EspP}-scSRP (Supplementary Fig. 6), HGSR in SPARX was applied with an angular step size of 7.5 degree to assign the data set into 377 angular regions. This resulted in 23 2D–projection images per stratum. With 90% of data retained in least populated strata, each resampled volume was generated from a set of 8,671 projections (21.4% of total data set) and a total of 9,990 re-sampled volumes were generated with these settings.

The average and variance (sxvar.py of SPARX) were obtained for the 15 Å low-pass-filtered, re-sampled volumes for the data set. Supplementary Figure 6 shows the 3D average map of all re-sampled volumes for RNC^{EspP}-scSRP coloured by their variance. The color code is based on the voxel values of the variance map.

In Xmipp, the data was split randomly into 10 parts with which 10 initial volumes were calculated using the angles from an alignment against a vacant, low pass filtered not-ratcheted ribosome[53]. The resulting volumes were compared, and based on differences in the SRP-FtsY density, three volumes were chosen for simultaneous 3D multi-reference refinement and classification in mlf_refine3d. The multi-reference refinement was converged after 20 iterations. Visual inspection of these volumes indicated the existence of at least two clearly distinct SRP-FtsY conformations showing differences in the Ffh M-domain and in the Ffh-FtsY NG-domain arrangement. Furthermore, these three volumes were used as initial models for supervised classification using SPIDER resulting in two very similar volumes and a third markedly different volume. The two sub-pools after 3 rounds of supervised classification contained 19,292 and 21,282 particles showing clear differences in the SRP-FtsY conformation (Supplementary Fig. 7).

Generation of the Quasi-Atomic Model

The crystal structure of the *E. coli* 70S ribosome[30] was fitted into the EM map with UCSF Chimera[59]. The atomic model of the *E. coli* SRP-FtsY complex was generated using the crystal structures of (1) the *E. coli* 4.5S RNA[23], of (2) the *Sulfolobus solfataricus* Ffh M-

domain with the yeast dipeptidyl aminopeptidase signal sequence[8] which fitted our density better (correlation coefficient 0.152) as compared to the *Methanococcus jannaschii* M-domain with an idealized signal sequence (cc of 0.148)[9], and of (3,4) the Ffh and FtsY NG-domains[6,10]. The domains were placed as rigid bodies into the EM density using UCSF Chimera [59]. The resulting model was energy minimized in CNS Version 1.0[60]. The figures were generated with PyMOL (DeLano Scientific).

Protein Targeting and Translocation Assay

The signal sequences of EspP and variants (Fig. 1a) were fused N-terminally to the signal peptidase cleavage site and to the mature region of pre-Prolactin. Their respective targeting efficiencies were determined by a co-translational protein targeting and translocation assay in the presence of SRP, FtsY and endoplasmatic reticulum microsomes, as described previously[34]. To accurately determine targeting efficiency and to avoid a bottleneck in the translocation step, Prolactin was chosen as a model substrate rather than the EspP protein because its translocation is highly efficient across the membrane and thus is not rate-limiting for the observed reaction. For the same reason, microsomal membranes were used for this assay because they are more active in *in vitro* translocation compared to *E. coli* membranes. Endogenous SRP and SRP receptor from microsomal membranes have been removed by high salt wash and trypsin digestion. Importantly, *E. coli* SRP and FtsY can mediate protein targeting in this assay as efficiently as the mammalian SRP and SRP receptor[33].

Fluorescence Measurements

Fluorescence measurements were carried out on a FluoroLog-3–22 spectrofluorometer (Jobin-Yvon) or an SF-2004 stopped-flow apparatus (KinTek). In experiments involving SRP-RNC complexes, saturating concentrations of RNCs (a factor of 50 or 100 above the respective K_d value) were used to ensure that >90% of SRP was bound with cargo. All reactions were carried out at 25 °C in assay buffer (50 mM KHEPES pH 7.5, 150 mM KOAc, 10 mM $Mg(OAc)_2$, 2 mM DTT and 10% glycerol).

The binding affinities of SRP for RNCs were determined using fluorescence anisotropy as described [15]. Equilibrium titrations were carried out with 5–10 nM of fluorescein-labeled Ffh(C421) and varying concentrations of RNC. Observed anisotropy values (A) are fit to equation 1,

$$A = A_0 + (A_1 - A_0)\left\{\frac{[\mathrm{SRP}]+[\mathrm{RNC}]+K_d - \sqrt{([\mathrm{SRP}]+[\mathrm{RNC}]+K_d)^2 - 4[\mathrm{SRP}][\mathrm{RNC}]}}{2[\mathrm{SRP}]}\right\} \quad (1)$$

in which A_0 is the anisotropy value of free SRP, A_1 is the anisotropy value when SRP is bound to cargo, and K_d is the equilibrium dissociation constant of SRP for the RNC.

Equilibrium titrations of the *early* intermediate were carried out using FRET between donor (DACM)-labeled SRP(C235) and acceptor (BODIPY-FL)-labeled FtsY(C487), respectively, as described previously[35]. Rate constants for rearrangement of the *early* intermediate to the *closed* complex were measured using SRP-C235 labeled with acrylodan. An RNC-SRP-FtsY *early* intermediate was preformed in the presence of saturating SRP and FtsY with respect to the K_d value of the *early* intermediate. The reaction was initiated by mixing 500 mM GppNHp with the *early* intermediate. The time course of fluorescence change was fit to single-exponential functions to give the rearrangement rate constants.

Association rate constants for SRP–FtsY *closed* complex formation were determined using FRET as described previously[19]. Complex assembly was initiated by mixing SRP with

varying amounts of FtsY in the presence of 100 μM GppNHp, and the time course of fluorescence change was monitored, giving the observed rate constants for SRP-FtsY binding (k_{obsd}). Linear fits (eq 2) of the observed rate constants were plotted as a function of FtsY concentration to give the second-order association rate constant, k_{on}.

$$k_{obsd}=k_{on}[\mathrm{Fts\ \ Y}]+k_{off} \quad (2)$$

Supplementary Material

Refer to Web version on PubMed Central for supplementary material.

Acknowledgments

We thank Dr. T. Shaikh for advice with Spider refinement and Dr. P. Penczek for assistance with SPARX. We thank Dr. M. Bacia for excellent technical assistance and the protein expression facility at EMBL Heidelberg as well as the Partnership for Structural Biology in Grenoble for support. The Polara microscope is part of the IBS Structural Biology and Dynamics GIS-IBISA-labeled platform. C.S. acknowledges support by the Agence Nationale de la Recherche (JC09_471873), the region Rhône-Alpes (CIBLE_1976) and the European Research Council by an ERC Starting grant (project 281331). K.K. was supported by a postdoctoral EMBO fellowship. We thank I. Saraogi in the Shan lab for sharing unpublished results and for critical reading of the manuscript. S.S. is supported by US National Institutes of Health (NIH) grant R01 GM078024, and the Fellowship for science and engineering from the David and Lucile Packard foundation. A.A. was supported by the US National Institute of General Medical Sciences (NIGMS) Ruth L. Kirschstein National Research Service Award (F31GM095294) and the NIH/ National Research Service Award (NRSA) Training Grant 5T32GM07616. X.Z. is a Howard Hughes Medical Institute Fellow of the Helen Hay Whitney Foundation.

MAIN TEXT REFERENCES

1. Gilmore R, Walter P, Blobel G. Protein translocation across the endoplasmic reticulum. II. Isolation and characterization of the signal recognition particle receptor. J. Cell Biol. 1982; 95:470–477. [PubMed: 6292236]
2. Keenan RJ, Freymann DM, Stroud RM, Walter P. The signal recognition particle. Annu. Rev. Biochem. 2001; 70:755–775. [PubMed: 11395422]
3. Nagai K, et al. Structure, function and evolution of the signal recognition particle. EMBO J. 2003; 22:3479–3485. [PubMed: 12853463]
4. Doudna JA, Batey RT. Structural insights into the signal recognition particle. Annu. Rev. Biochem. 2004; 73:539–557. [PubMed: 15189152]
5. Poritz MA, et al. An *E. coli* ribonucleoprotein containing 4.5S RNA resembles mammalian signal recognition particle. Science. 1990; 250:1111–1117. [PubMed: 1701272]
6. Freymann DM, Keenan RJ, Stroud RM, Walter P. Structure of the conserved GTPase domain of the signal recognition particle. Nature. 1997; 385:361–364. [PubMed: 9002524]
7. Batey RT, Rambo RP, Lucast L, Rha B, Doudna JA. Crystal structure of the ribonucleoprotein core of the signal recognition particle. Science. 2000; 287:1232–1239. [PubMed: 10678824]
8. Janda CY, et al. Recognition of a signal peptide by the signal recognition particle. Nature. 2010; 465:507–510. [PubMed: 20364120]
9. Hainzl T, Huang S, Merilainen G, Brannstrom K, Sauer-Eriksson AE. Structural basis of signal-sequence recognition by the signal recognition particle. Nat. Struct. Mol. Biol. 2011; 18:389–391. [PubMed: 21336278]
10. Montoya G, Svensson C, Luirink J, Sinning I. Crystal structure of the NG domain from the signal-recognition particle receptor FtsY. Nature. 1997; 385:365–368. [PubMed: 9002525]
11. Angelini S, Deitermann S, Koch HG. FtsY, the bacterial signal-recognition particle receptor, interacts functionally and physically with the SecYEG translocon. EMBO Rep. 2005; 6:476–481. [PubMed: 15815684]
12. Weiche B, et al. A cleavable N-terminal membrane anchor is involved in membrane binding of the *Escherichia coli* SRP receptor. J. Mol. Biol. 2008; 377:761–773. [PubMed: 18281057]

13. Egea PF, et al. Substrate twinning activates the signal recognition particle and its receptor. Nature. 2004; 427:215–221. [PubMed: 14724630]
14. Focia PJ, Shepotinovskaya IV, Seidler JA, Freymann DM. Heterodimeric GTPase core of the SRP targeting complex. Science. 2004; 303:373–377. [PubMed: 14726591]
15. Zhang X, Rashid R, Wang K, Shan SO. Sequential checkpoints govern substrate selection during cotranslational protein targeting. Science. 2010; 328:757–760. [PubMed: 20448185]
16. Holtkamp W, et al. Dynamic switch of the signal recognition particle from scanning to targeting. Nat. Struct. Mol. Biol. 2012; 19:1332–1337. [PubMed: 23142984]
17. Halic M, et al. Following the signal sequence from ribosomal tunnel exit to signal recognition particle. Nature. 2006; 444:507–511. [PubMed: 17086193]
18. Peluso P, Shan SO, Nock S, Herschlag D, Walter P. Role of SRP RNA in the GTPase cycles of Ffh and FtsY. Biochemistry. 2001; 40:15224–15233. [PubMed: 11735405]
19. Zhang X, Schaffitzel C, Ban N, Shan SO. Multiple conformational switches in a GTPase complex control co-translational protein targeting. Proc. Natl. Acad. Sci. USA. 2009; 106:1754–1759. [PubMed: 19174514]
20. Estrozi LF, Boehringer D, Shan SO, Ban N, Schaffitzel C. Structure of the *E. coli* Co-translational Targeting Complex in the Stable *Early* Conformation. Nat. Struct. Mol. Biol. 2011; 18:88–90. [PubMed: 21151118]
21. Lam VQ, Akopian D, Rome M, Henningsen D, Shan SO. Lipid activation of the signal recognition particle receptor provides spatial coordination of protein targeting. J. Cell Biol. 2010; 190:623–635. [PubMed: 20733058]
22. Shen K, Arslan S, Akopian D, Ha T, Shan SO. Activated GTPase movement on an RNA scaffold drives co-translational protein targeting. Nature. 2012; 492:271–275. [PubMed: 23235881]
23. Ataide SF, et al. The crystal structure of the signal recognition particle in complex with its receptor. Science. 2011; 331:881–886. [PubMed: 21330537]
24. Connolly T, Rapiejko P, Gilmore R. Requirement of GTP hydrolysis for dissociation of the signal recognition particle from its receptor. Science. 1991; 252:1171–1173. [PubMed: 1851576]
25. Tian H, Boyd D, Beckwith J. A mutant hunt for defects in membrane protein assembly yields mutations affecting the bacterial signal recognition particle and Sec machinery. Proc. Natl. Acad. Sci. USA. 2000; 97:4730–4735. [PubMed: 10781078]
26. Valent QA, et al. Early events in preprotein recognition in *E. coli*: interaction of SRP and trigger factor with nascent polypeptides. EMBO J. 1995; 14:5494–5505. [PubMed: 8521806]
27. Lee HC, Bernstein HD. The targeting pathway of *Escherichia coli* presecretory and integral membrane proteins is specified by the hydrophobicity of the targeting signal. Proc. Natl. Acad. Sci. USA. 2001; 98:3471–3476. [PubMed: 11248102]
28. Peterson JH, Szabady RL, Bernstein HD. An unusual signal peptide extension inhibits the binding of bacterial presecretory proteins to the signal recognition particle, trigger factor, and the SecYEG complex. J. Biol. Chem. 2006; 281:9038–9048. [PubMed: 16455668]
29. Szabady RL, Peterson JH, Skillman KM, Bernstein HD. An unusual signal peptide facilitates late steps in the biogenesis of a bacterial autotransporter. Proc. Natl. Acad. Sci. USA. 2005; 102:221–226. [PubMed: 15615856]
30. Schuwirth BS, et al. Structures of the bacterial ribosome at 3.5 A resolution. Science. 2005; 310:827–834. [PubMed: 16272117]
31. Rosendal KR, Wild K, Montoya G, Sinning I. Crystal structure of the complete core of archaeal signal recognition particle and implications for interdomain communication. Proc. Natl. Acad. Sci. USA. 2003; 100:14701–14706. [PubMed: 14657338]
32. Schaffitzel C, et al. Structure of the *E. coli* signal recognition particle bound to a translating ribosome. Nature. 2006; 444:503–506. [PubMed: 17086205]
33. Powers T, Walter P. Co-translational protein targeting catalyzed by the *Escherichia coli* signal recognition particle and its receptor. EMBO J. 1997; 16:4880–4886. [PubMed: 9305630]
34. Shan SO, Chandrasekar S, Walter P. Conformational changes in the GTPase modules of the signal reception particle and its receptor drive initiation of protein translocation. J. Cell Biol. 2007; 178:611–620. [PubMed: 17682051]

35. Zhang X, Kung S, Shan SO. Demonstration of a multistep mechanism for assembly of the SRP x SRP receptor complex: implications for the catalytic role of SRP RNA. J. Mol. Biol. 2008; 381:581–593. [PubMed: 18617187]
36. Braig D, et al. Signal sequence-independent SRP-SR complex formation at the membrane suggests an alternative targeting pathway within the SRP cycle. Mol. Biol. Cell. 2011; 22:2309–2323. [PubMed: 21551068]
37. Shen K, Shan SO. Transient tether between the SRP RNA and SRP receptor ensures efficient cargo delivery during cotranslational protein targeting. Proc. Natl. Acad. Sci. USA. 2010; 107:7698–7703. [PubMed: 20385832]
38. Scheres SH, et al. Disentangling conformational states of macromolecules in 3D–EM through likelihood optimization. Nat. Methods. 2007; 4:27–29. [PubMed: 17179934]
39. Shaikh TR, et al. SPIDER image processing for single-particle reconstruction of biological macromolecules from electron micrographs. Nat. Protoc. 2008; 3:1941–1974. [PubMed: 19180078]
40. Zhang X, et al. Direct visualization reveals dynamics of a transient intermediate during protein assembly. Proc. Natl. Acad. Sci. USA. 2011; 108:6450–6455. [PubMed: 21464281]
41. Knoops K, Schoehn G, Schaffitzel C. Cryo-electron microscopy of ribosomal complexes in cotranslational folding, targeting, and translocation. Wiley Interdiscip. Rev. RNA. 2011; 3:429–441. [PubMed: 22095783]
42. Cross BC, Sinning I, Luirink J, High S. Delivering proteins for export from the cytosol. Nat. Rev. Mol. Cell Biol. 2009; 10:255–264. [PubMed: 19305415]
43. Bradshaw N, Neher SB, Booth DS, Walter P. Signal sequences activate the catalytic switch of SRP RNA. Science. 2009; 323:127–130. [PubMed: 19119234]
44. Peterson JH, Woolhead CA, Bernstein HD. The conformation of a nascent polypeptide inside the ribosome tunnel affects protein targeting and protein folding. Mol. Microbiol. 2010; 78:203–217. [PubMed: 20804452]
45. Raine A, et al. Targeting and insertion of heterologous membrane proteins in. E. coli. Biochimie. 2003; 85:659–668.
46. Flanagan JJ, et al. Signal recognition particle binds to ribosome-bound signal sequences with fluorescence-detected subnanomolar affinity that does not diminish as the nascent chain lengthens. J. Biol. Chem. 2003; 278:18628–18637. [PubMed: 12621052]
47. Miyazaki E, Kida Y, Mihara K, Sakaguchi M. Switching the sorting mode of membrane proteins from cotranslational endoplasmic reticulum targeting to posttranslational mitochondrial import. Mol. Biol. Cell. 2005; 16:1788–1799. [PubMed: 15673615]
48. del Alamo M, et al. Defining the specificity of cotranslationally acting chaperones by systematic analysis of mRNAs associated with ribosome-nascent chain complexes. PLoS Biol. 2011; 9:e1001100. [PubMed: 21765803]
49. Lauring B, Sakai H, Kreibich G, Wiedmann M. Nascent polypeptide-associated complex protein prevents mistargeting of nascent chains to the endoplasmic reticulum. Proc. Natl. Acad. Sci. USA. 1995; 92:5411–5415. [PubMed: 7777521]

ONLINE METHODS REFERENCES

50. Schaffitzel C, Ban N. Generation of ribosome nascent chain complexes for structural and functional studies. J. Struct. Biol. 2007; 158:463–471. [PubMed: 17350284]
51. Heymann JB, Belnap DM. Bsoft: image processing and molecular modeling for electron microscopy. J. Struct. Biol. 2007; 157:3–18. [PubMed: 17011211]
52. Tang G, et al. EMAN2: an extensible image processing suite for electron microscopy. J. Struct. Biol. 2007; 157:38–46. [PubMed: 16859925]
53. Valle M, et al. Incorporation of aminoacyl-tRNA into the ribosome as seen by cryo-electron microscopy. Nat. Struct. Biol. 2003; 10:899–906. [PubMed: 14566331]
54. Valle M, et al. Locking and unlocking of ribosomal motions. Cell. 2003; 114:123–134. [PubMed: 12859903]

55. Fischer N, Konevega AL, Wintermeyer W, Rodnina MV, Stark H. Ribosome dynamics and tRNA movement by time-resolved electron cryomicroscopy. Nature. 2010; 466:329–333. [PubMed: 20631791]

56. Rosenthal PB, Henderson R. Optimal determination of particle orientation, absolute hand, and contrast loss in single-particle electron cryomicroscopy. J. Mol. Biol. 2003; 333:721–745. [PubMed: 14568533]

57. Scheres SH, Nunez-Ramirez R, Sorzano CO, Carazo JM, Marabini R. Image processing for electron microscopy single-particle analysis using XMIPP. Nat. Protoc. 2008; 3:977–990. [PubMed: 18536645]

58. Penczek PA, Kimmel M, Spahn CM. Identifying conformational states of macromolecules by eigen-analysis of resampled cryo-EM images. Structure. 2011; 19:1582–1590. [PubMed: 22078558]

59. Pettersen EF, et al. UCSF Chimera--a visualization system for exploratory research and analysis. J. Comput. Chem. 2004; 25:1605–1612. [PubMed: 15264254]

60. Brunger AT, et al. Crystallography & NMR system: A new software suite for macromolecular structure determination. Acta Crystallogr. D Biol. Crystallogr. 1998; 54:905–921. [PubMed: 9757107]

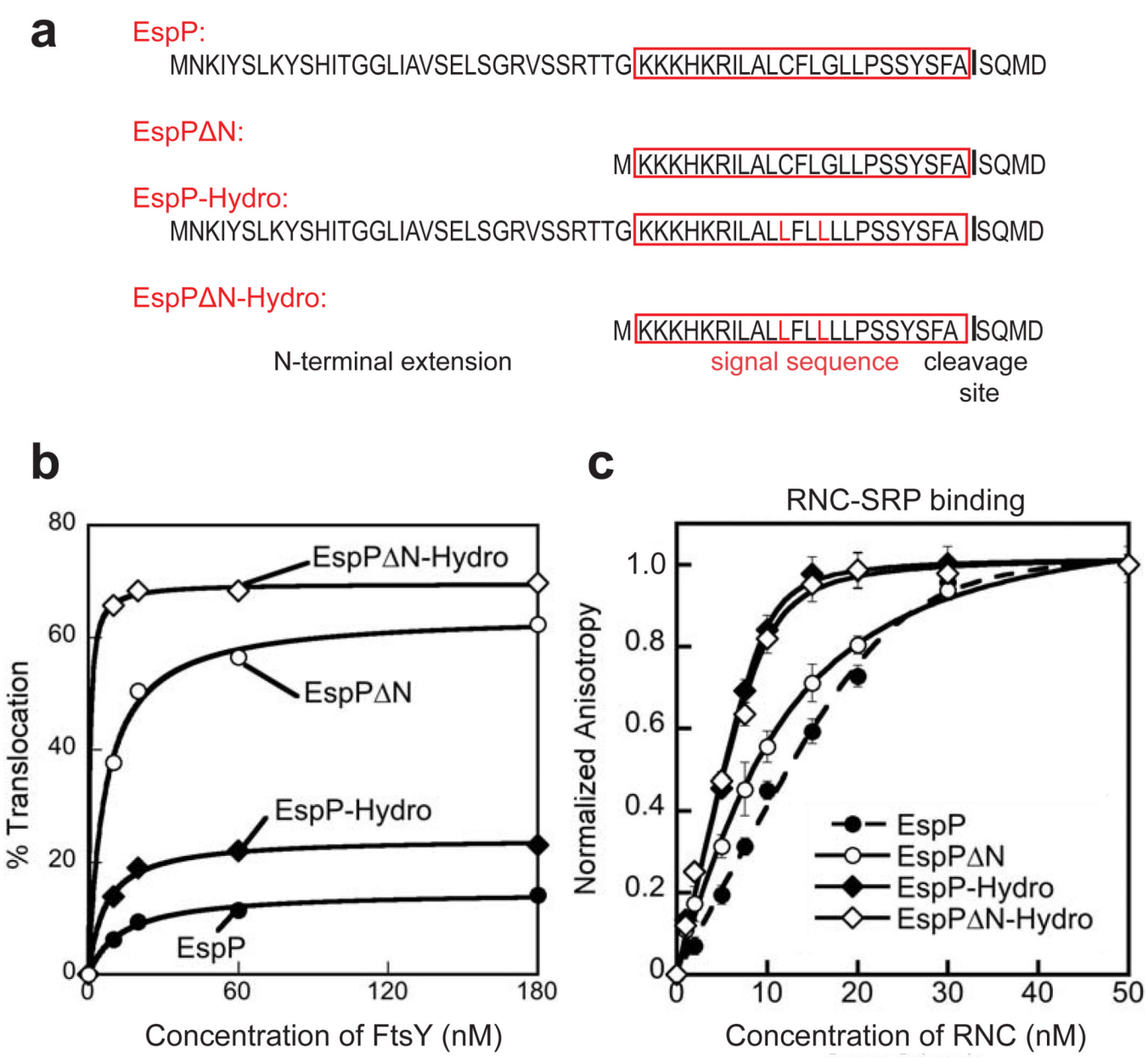

Figure 1. The N-terminal extension of EspP inhibits co-translational protein targeting but does not affect RNC-SRP binding

(a) Signal sequences of EspP and its variants used in this study. The N-terminal extension of the signal sequence and the signal peptide cleavage site are indicated. The classical signal sequence is marked by a red box, and mutations are highlighted by red letters. **(b)***In vitro* targeting and translocation efficiency of EspP signal sequence variants fused to Prolactin using microsomal membranes. **(c)** Equilibrium titration of RNC-SRP binding. Error bars represent standard deviation, with n = 3..

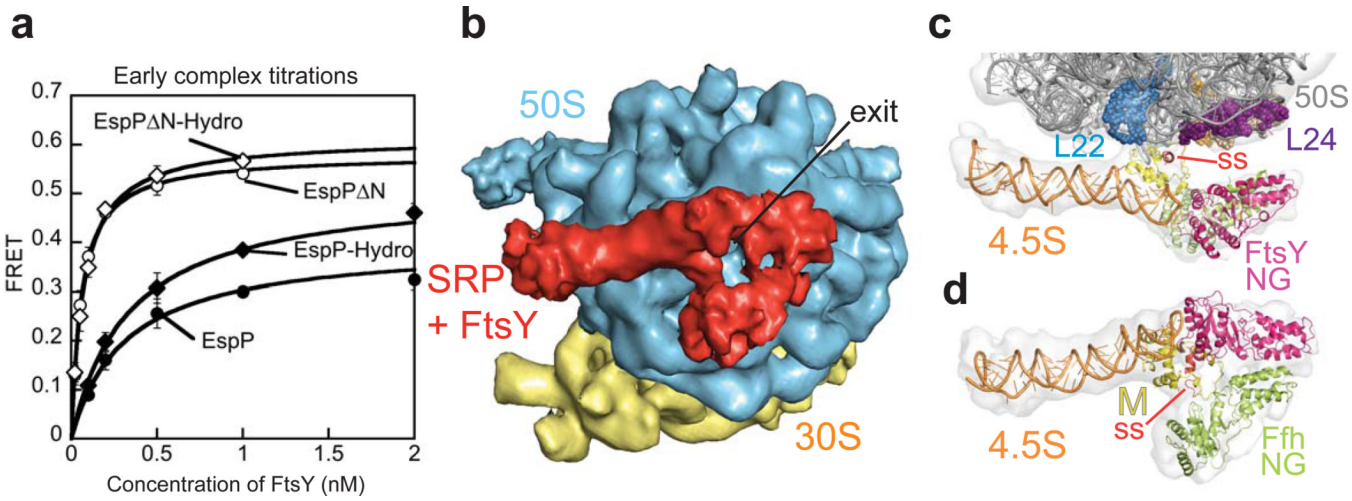

Figure 2. The EspPN-terminal extension leads to a weaker and distorted *early* targeting complex

(a) Equilibrium titration of the SRP•FtsY *early* complex in the presence of RNCs bearing EspP signal sequence variants. 300–500 nM RNCs were used to ensure that most of the SRP is ribosome-bound. Error bars represent standard deviation, with n = 3. (**b**) Cryo-EM structure of RNC^{EspP}-SRP-FtsY shown with the view into the polypeptide exit tunnel. The large ribosomal subunit (50S) is depicted in blue, the small ribosomal subunit (30S) in yellow and the single chain SRP-FtsY in red. **(c,d)** EM reconstruction and quasi-atomic model of the RNC^{EspP}-SRP-FtsY *early* complex **(c)** in a close-up view from the back of the 50S subunit and **(d)** in a view as in (b). The experimental density is shown in light grey, 4.5S RNA in orange, the EspP signal sequence (ss) in red, the Ffh M-domain in yellow, the Ffh NG-domain in greenyellow, the FtsY NG-domain in magenta, the 50S rRNA in dark gray, ribosomal proteins L24 in purple and L22 in skyblue. The density of the ribosome is not shown in (d) for clarity.

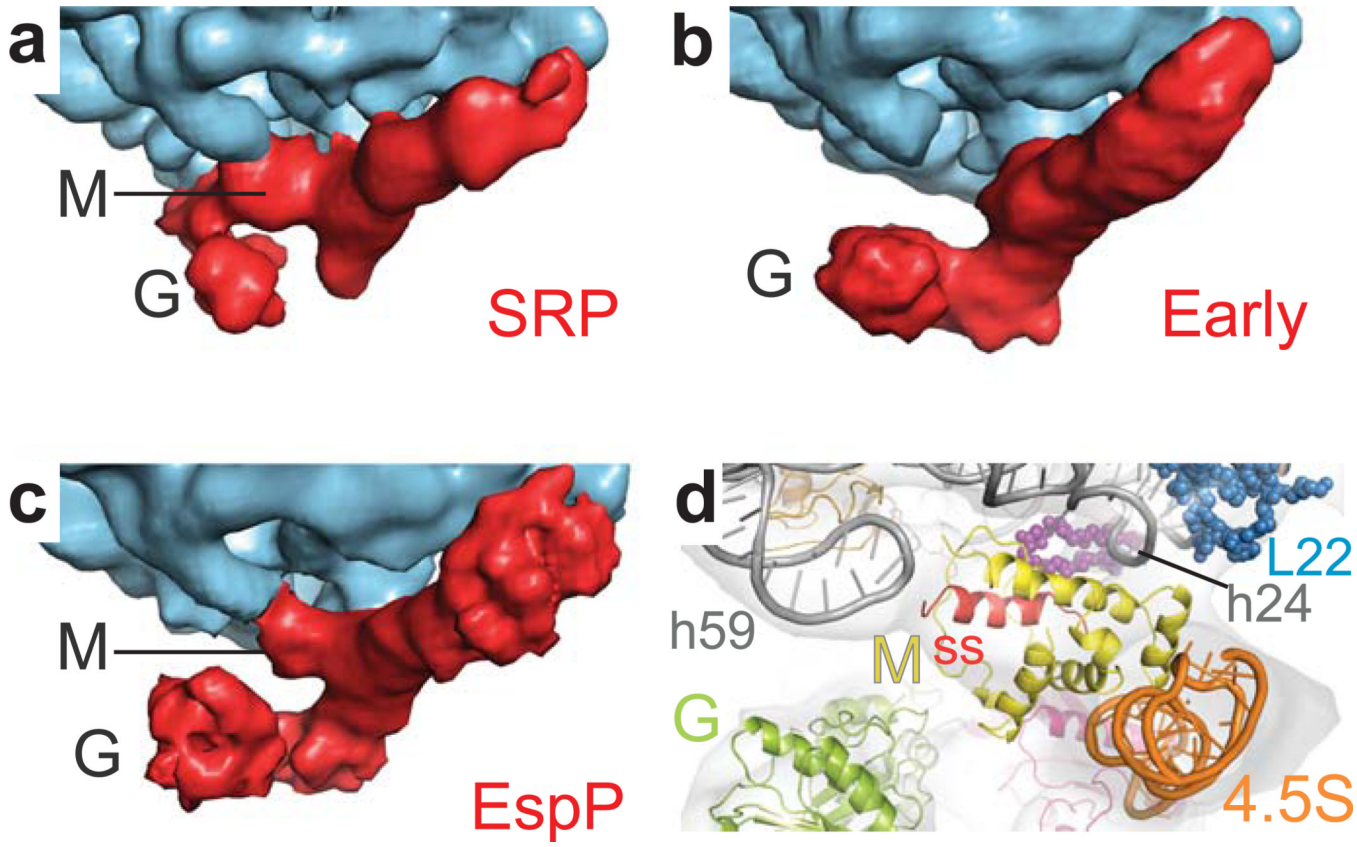

Figure 3. M-domain arrangement during co-translational targeting

(a) Close-up view on the exit of the ribosomal tunnel and the M-domain of the RNC^{FtsQ}-SRP cryo-EM structure[17]. Color coding is the same as in Figure 2c. **(b)** Same view as in (a) for the RNC^{FtsQ}-SRP-FtsY *early* complex[20]. **(c)** Cryo-EM structure of the RNC^{EspP}-SRP-FtsY *early* complex shown in the same view as (a,b) for comparison. **(d)** Close-up on the M-domain with the signal sequence in the EM reconstruction and quasi-atomic model of the RNC^{EspP}-SRP-FtsY complex. Color coding is the same as in Figure 2d,e. The positions of the Ffh M- and G-domains are indicated.

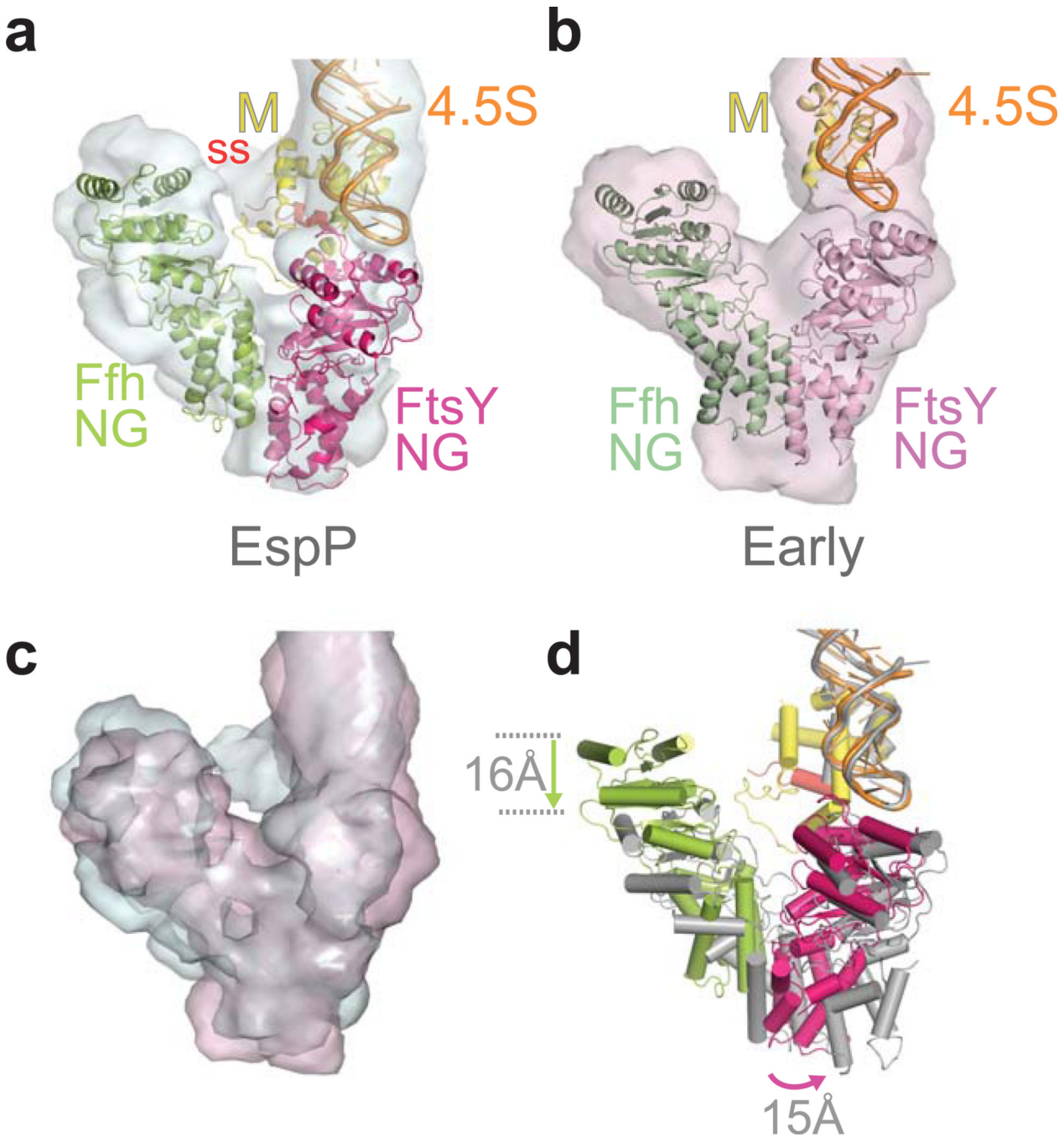

Figure 4. Ffh-FtsY NG-domain arrangement in the 'false' *early* complex formed with EspP compared to the productive *early* complex formed with a correct cargo

(a) In the RNC^{EspP}•SRP•FtsY 'false' *early* complex, the Ffh-FtsY NG-domains have a weak interface involving the N-domain of Ffh and the NG-domain of FtsY. The experimental density is depicted in pale cyan; unfilled density indicates flexibility in this part. **(b)** Pseudo-symmetric V-shaped NG-domain arrangement in the *early* targeting complex with $RNC^{FtsQ\ 20}$. The experimental density of this complex is shown in light pink. **(c,d)** Overlays of **(c)** the EM densities of the *early* targeting complexes from (a) & (b), and **(d)** the corresponding quasi-atomic models. Arrows indicate positional differences of the NG-domains. For the overlays (c,d), the RNA tetraloops of the structures (c) and models (d)

have been aligned. Color codings of the quasi-atomic models are as in Figure 2 except in (d), where the NG-domain complex of the *early* targeting complex with RNC^{FtsQ} is depicted in grey for clarity.

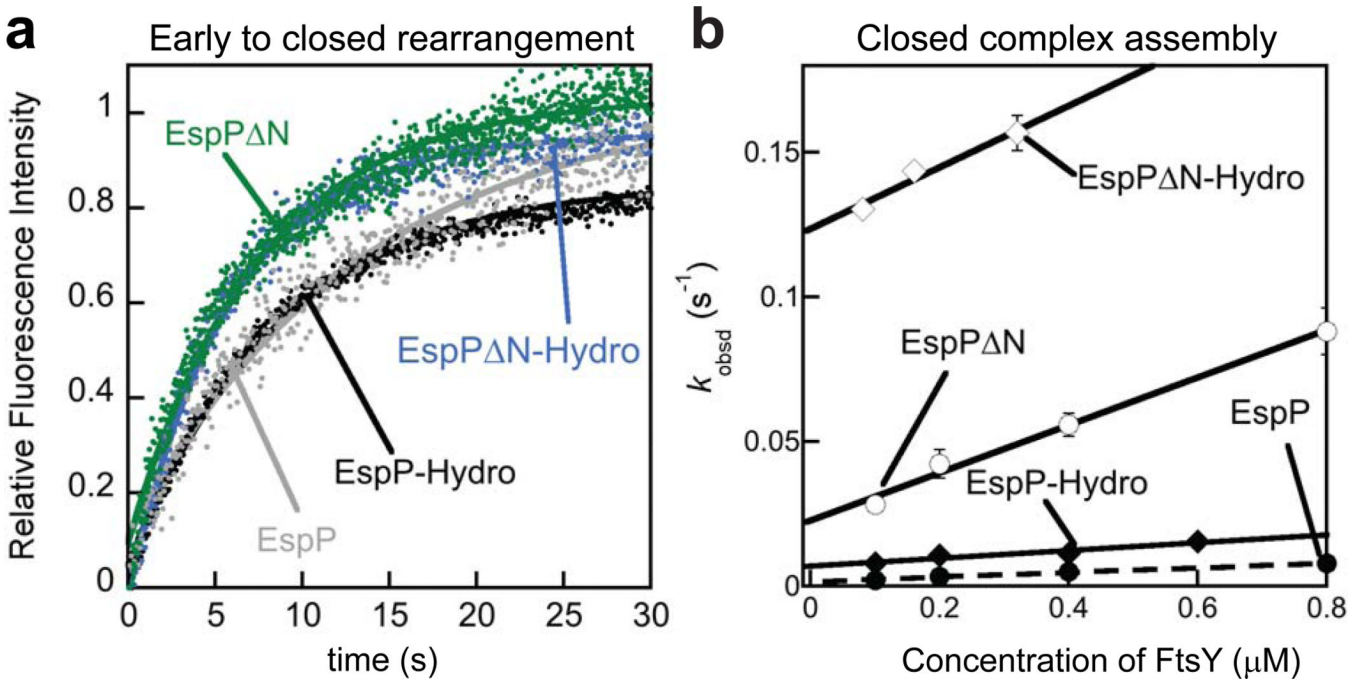

Figure 5. The N-terminal extension leads to a less productive *early* complex and slower assembly of the *closed* SRP-FtsY complex

(a) Kinetics for rearrangement of the *early* to the *closed* complex for EspP [15] and variants. **(b)** Assembly rates of the *closed* SRP-FtsY complex mediated by RNCs displaying EspP signal sequence variants. Error bars represent standard deviation, with n = 4.

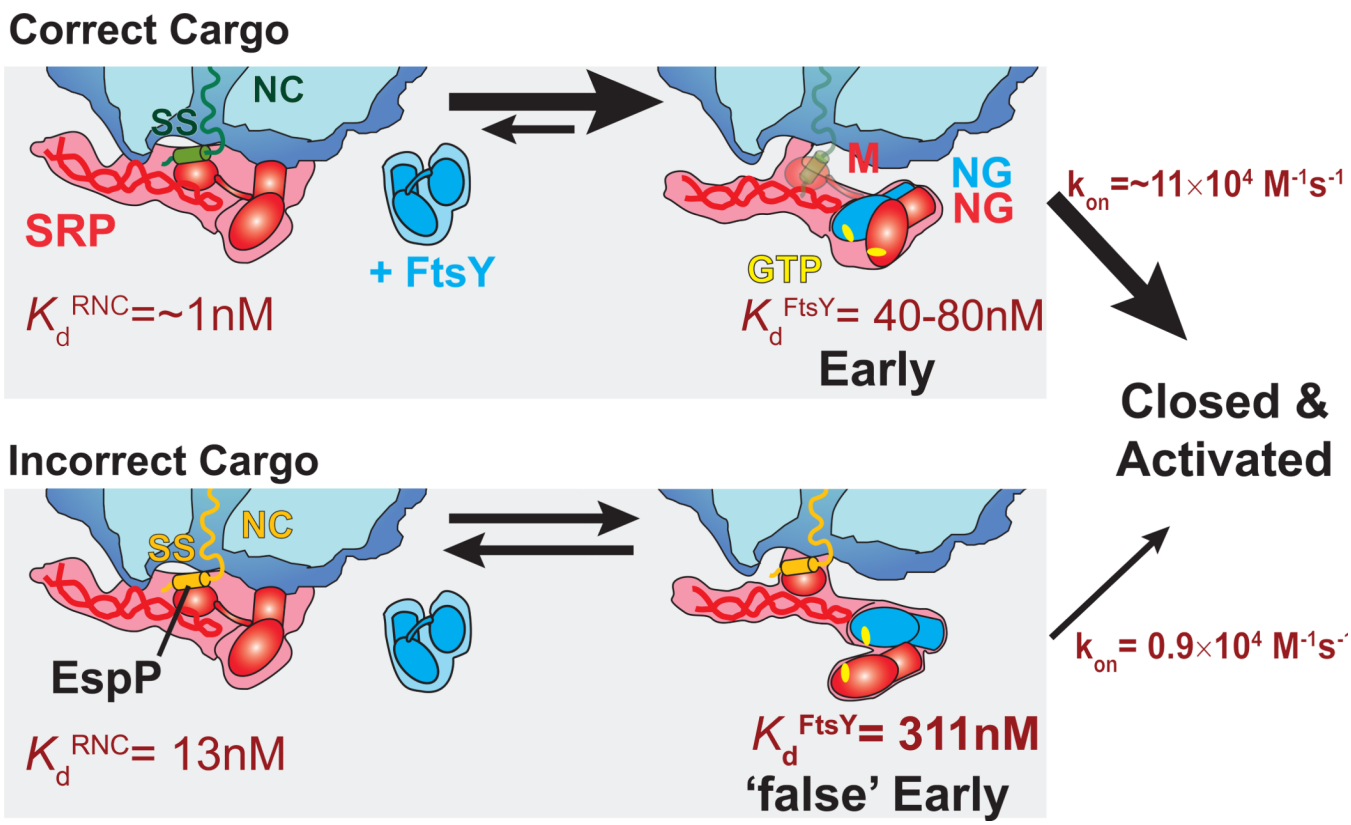

Figure 6. Model of signal sequence surveillance by the SRP and FtsY

The SRP tightly binds to correct cargos. FtsY binding leads to detachment of SRP from the ribosome, and a pseudo-symmetric NG-domain arrangement. EspP has a less hydrophobic signal sequence, leading to a moderate affinity of SRP (13 nM). FtsY has a lower affinity (311 nM) for this SRP-RNC^{EspP} complex and forms a less favourable, distorted and flexible Ffh-FtsY NG-domain heterodimer. The EspP 'false' *early* targeting complex NG-domains that are loosely associated and rearrange inefficiently into the *closed/activated* state leading to premature FtsY dissociation rather than successful completion of the targeting reaction.

Table 1

Interaction parameters of complexes formed by RNC, SRP and FtsY, and resulting translocation efficiency

This table summarizes the results derived from experiments shown in Figure 1b,c, in Figure 2a and in Figure 5a,b. Values represent mean ±SD.

	RNC-SRP K_d (nM)	Early complex K_d (nM)	Early complex FRET	Early-to-closed rearrangement $k_{e\rightarrow c}$ (s^{-1})	Closed complex assembly rate $k_{on}\times10^3$ ($M^{-1}s^{-1}$)	% Translocation
EspP	13.6 ± 1.2	311 ± 11	0.39 ± 0.02	0.04 ± 0.01	9.2 ± 1.1	15.8 ± 1.2
EspPΔN	13.4 ± 0.78	58 ± 10	0.55 ± 0.01	0.13 ± 0.01	91.2 ± 7.8	66.7 ± 5.3
EspP Hydro	1.0 ± 0.05	300 ± 4	0.51 ± 0.01	0.10 ± 0.01	15.2 ± 1.2	22.8 ± 2.0
EspPΔN Hydro	1.0 ± 0.3	42 ± 5	0.61 ± 0.02	0.18 ± 0.02	112 ± 5.3	68.3 ± 1.9